Automotive Science and Engineering, Vol. 16, No. 3, (2026), 5189-5207

Iran University of Science and Technology

Automotive Science and Engineering

Journal Homepage: ase.iust.ac.ir

ISSN: 2008-9899

# Investigation of a Novel Heat Pipe-Assisted Composite for Thermal Management of Prismatic Cells

**Ma. Babalooei-noori[1], A. Alinia-ziazi[1*], G.R. Molaeimanesh[2], S. Etemadi Haghighi[1]**

[1] Department of Mechanical Engineering, SR.C., Islamic Azad University, Tehran, Iran

[2] School of Automotive Engineering, Iran University of Science and Technology, Tehran, Iran

**ARTICLE INFO**

**Article history**:

Received : 26 Jan 2026

Accepted: 21 Aug 2026

Published: 26 Sep 2026

**Keywords**:

Battery Thermal Management System (BTMS)

Prismatic Cell

Phase Change Material (PCM)

Composite

Heat Pipe

Copper Foam

**A B S T R A C T**

The thermal management of prismatic lithium-ion battery cells under high heat fluxes remains a critical challenge for electric vehicle safety and lifespan. Excessive heat generation can lead to thermal runaway, capacity fade, and reduced battery life. This study numerically investigates the thermal performance of a hybrid battery thermal management system (BTMS) integrating a paraffin-based composite and a flat heat pipe. The working hypothesis is that the combined effects of latent heat storage in the PCM and rapid heat transport by the heat pipe can effectively buffer transient thermal loads. A three-dimensional transient CFD model was developed in ANSYS Fluent, using the enthalpy-porosity method for PCM melting and the equivalent thermal conductivity approach for the heat pipe. The effects of applied heat flux (1000–5000 W/m²) and condenser convective heat transfer coefficient (5–500 W/(m²·K)) on cell temperature, temperature uniformity, PCM liquid fraction, and apparent thermal resistance were systematically evaluated. The results show that increasing heat flux significantly increases cell temperature and accelerates PCM melting. At $q'' = 5000\ \mathrm{W/m^2}$ and $h = 50\ \mathrm{W/(m^2 \cdot K)}$, melting onset advanced from 290 s to 45 s, and complete melting occurred at 145 s, whereas at $q'' = 1000\ \mathrm{W/m^2}$, only 35% of the PCM melted within 600 s. The maximum cell temperature reached approximately 400 K at $h = 5\ \mathrm{W/(m^2 \cdot K)}$ but decreased to 315 K at $h = 500\ \mathrm{W/(m^2 \cdot K)}$, demonstrating the critical role of effective external cooling. The maximum temperature difference between the cell and composite ranged from 0.1 to 3.0 K, while the apparent thermal resistance varied between 0.02 and 0.21 K/W. Overall, the hybrid configuration effectively controls battery temperature through combined latent heat storage and heat-pipe heat transport, with performance strongly dependent on both heat flux and convective cooling. These findings provide valuable insights for the design of passive BTMS in high-power battery applications.

*Corresponding Author
Email Address: ali_alinia@iau.ac.ir
https://doi.org/10.22068/ase.2026.753

"*Automotive Science and Engineering*" is licensed under a Creative Commons Attribution-Noncommercial 4.0 International License.

[ Downloaded from ahc.iust.ac.ir on 2026-11-28 ]

## 1. Introduction

The rapid global transition toward electric vehicles (EVs) has been driven by the urgent need to reduce greenhouse gas emissions and dependence on fossil fuels. Lithium-ion batteries, owing to their high energy density and long cycle life, have become the dominant energy storage technology for EV powertrains. However, the performance, safety, and lifespan of lithium-ion batteries are strongly influenced by their operating temperature. Excessive heat generation during charging and discharging can lead to accelerated capacity fade, thermal runaway, and even catastrophic failure. Therefore, effective battery thermal management systems (BTMS) are essential for ensuring safe and reliable operation of lithium-ion batteries, particularly under high-rate discharge and high-temperature conditions [1], [2].

Various thermal management approaches have been proposed for controlling the temperature of lithium-ion batteries, including air cooling, liquid cooling, heat pipes, and phase change material (PCM)-based systems [3]. Among these methods, PCM-based thermal management has received considerable attention because of its ability to absorb and store a significant amount of thermal energy through latent heat during the phase transition. PCM systems can also provide passive thermal management without requiring continuous mechanical energy for fluid circulation, making them attractive for applications where simplicity, compactness, and low auxiliary power consumption are desired [4].

Despite these advantages, the practical application of conventional PCMs is limited by their relatively low thermal conductivity. Paraffin-based PCMs, which are widely used because of their suitable melting temperatures, chemical stability, relatively low cost, and high latent heat, generally exhibit poor thermal conductivity. This characteristic restricts the rate of heat propagation through the PCM and can lead to localized heat accumulation during periods of high battery heat generation [5]. Therefore, improving the thermal conductivity of paraffin while retaining its latent heat storage capability is essential for achieving an effective PCM-based BTMS [6].

One promising strategy for overcoming this limitation is the incorporation of highly conductive porous structures into the PCM. Metal foams can provide interconnected three-dimensional heat-conduction pathways and substantially enhance the effective thermal conductivity of the PCM [7]. At the same time, the porous structure provides a framework for accommodating the PCM within the composite structure. Previous studies have demonstrated that the integration of metallic foams with paraffin can significantly improve heat-transfer performance compared with pure PCM. For example, the incorporation of aluminum foam into paraffin-based PCM has been reported to increase the thermal conductivity from approximately 0.21 to 4.75 W/m·K [6].

Copper foam is particularly promising for this purpose because of its high thermal conductivity and interconnected porous structure. When paraffin is impregnated into copper foam, the copper skeleton acts as a highly conductive network through which heat can be rapidly transported from the heat-generating battery toward the PCM. The resulting copper-foam/paraffin composite can therefore provide a more effective combination of sensible and latent heat transfer than pure paraffin. In addition, previous investigations have indicated that the thermal performance of PCM/metal-foam composites is strongly affected by the characteristics of the porous structure, including porosity and pore density or pores per inch (PPI). These parameters influence the amount of metallic material, PCM volume fraction, effective thermal conductivity, heat storage capacity, and the overall heat-transfer behavior of the composite [8].

Although copper-foam/PCM composites can substantially improve thermal conduction, PCM-based systems remain fundamentally dependent on the rate at which heat can be transferred away from the battery and distributed within the thermal management structure. In this regard, heat pipes offer an attractive complementary technology. A heat pipe can rapidly transport thermal energy from a heated region to a remote



[ Downloaded from ahc.iust.ac.ir on 2026-11-28 ]

region through phase-change-driven heat transfer, while requiring no external mechanical pumping [4]. The combination of a highly conductive PCM composite with a heat pipe therefore provides the potential to simultaneously exploit the high heat-storage capability of PCM and the rapid heat-transport capability of a heat pipe.

The integration of these two thermal management mechanisms is particularly attractive for battery applications. The PCM can act as a thermal buffer by absorbing the transient heat generated by the battery, while the copper foam provides enhanced thermal conduction within the PCM composite [9]. Meanwhile, the heat pipe can facilitate the transfer of accumulated thermal energy away from the battery region. Such a hybrid configuration can potentially overcome some of the individual limitations of PCM- and heat-pipe-based cooling systems and provide improved control of battery temperature and temperature uniformity.

Despite the extensive research on PCM-based BTMSs and the growing interest in metal-foam-enhanced PCMs, limited attention has been given to combined configurations in which a multilayer PCM composite is integrated with a heat pipe for battery thermal management.

Feng et al. [10] conducted a comprehensive experimental and numerical study on a hybrid cooling system combining composite phase change material (CPCM) and flat heat pipes (HP) for battery thermal management. The thermal performance and applicable boundaries of the hybrid system were investigated through orthogonal tests under various operational and environmental conditions. The experimental results demonstrated that both the CPCM system and the CPCM-HP hybrid system could effectively control temperature rise and improve temperature uniformity. Compared to the air-cooling system, the maximum temperature in the hybrid system was 22 °C lower under a moderate thermal load at 25°C ambient temperature. The applicable boundary of the hybrid system was tested under a moderate thermal load at 40°C, where the maximum temperature exceeded the allowable range. The flat heat pipe provided excellent auxiliary heat dissipation for CPCM during cycling tests at 40 °C, making the maximum temperature 10 °C lower than the CPCM system and 15 °C lower than the air-cooling system. A lumped thermal model was developed and validated, and the effects of dimension size, copper foam porosity, and convective heat transfer coefficient on thermal performance were further analyzed. Based on the permitted temperature range, volume energy density, cooling performance, and operational circumstances, the best designs for these criteria were recommended.

Tang et al. [11] constructed a thermal management system consisting of paraffin/copper foam metal composite phase change material and heat pipe for lithium-ion battery packs. A one-dimensional electrochemical three-dimensional thermal coupling model was established, and the accuracy of the simulation model was verified by comparing with experimental data. Numerical simulations were performed on the operating voltage and temperature of lithium-ion battery packs under different charging rates and ambient temperatures. The results showed that copper foam-paraffin composite phase change material has the advantage of high thermal conductivity, and the heat pipe can disperse heat in time to ensure the temperature uniformity of the module. Compared with different thermal management systems, the study found that the system could control the module temperature rise and temperature difference at 5 °C and 0.7 °C under a low thermal load in a high-temperature environment. The cooling efficiency of the composite PCM-heat pipe coupling system was more efficient than that of natural cooling and composite PCM cooling. Through simulation verification, the system could meet the working requirements of modules under different environments and different charging rates. However, under the dual conditions of high temperature and high rate, refrigeration or liquid cooling coupling should be considered to assist management in the future. In addition, the influence of the size change of center distance between cells on system performance was studied, and a more suitable size range was given to meet the dual requirements of material

[ Downloaded from ahc.iust.ac.ir on 2026-11-28 ]

utilization rate and temperature control management.

Zhao et al. [12] investigated a hybrid battery thermal management system (BTMS) integrating phase change materials (PCMs) and heat pipes (HPs) for a 500 Ah pouch lithium iron phosphate battery through experiment and simulation. A thermoelectrically coupled simulation model was established using an improved hybrid pulse power characterization (HPPC) method. Various configurations of PCMs and HPs were analyzed under different thermal loads to obtain optimal arrangements. The results indicated that deploying HPs in high-temperature areas, particularly with direct contact, significantly improved thermal uniformity and reduced local high temperatures. To evaluate the system under extreme conditions, three consecutive charge-discharge cycles were conducted for both a battery and a three-battery module. The results demonstrated that under these extreme conditions, the temperature of the unmodified module peaked at 63.2 °C, whereas with the optimized BTMS configuration, the maximum temperature decreased to 49.0 °C, confirming the effectiveness of the hybrid BTMS. This study was particularly significant as it addressed large-capacity LIBs (500 Ah), which have received limited research attention in the BTMS literature, and provided valuable insights into the thermal management of large-format pouch cells with significant surface areas.

Zhang et al. [13] proposed a pure passive battery thermal management system coupled with heat pipe and expanded graphite-based composite phase change material (CPCM) for 18650 cylindrical lithium battery modules under high-rate discharge conditions. The performance difference between coupled cooling and single cooling strategy was compared, and the influence of heat pipe layout and expanded graphite (EG) content on the heat dissipation effect was explored under different working conditions. A technical and economic evaluation of the whole life cycle was also carried out. The results showed that the cooling effect of PCM was significantly better than that of natural cooling under low-to-high thermal loads, and the HP + PCM coupling system exhibited superior performance. The temperature rise rate under high thermal load was 84.1% lower than that of natural cooling, the maximum temperature was 5.13% lower than that of the pure PCM system, and the temperature uniformity of the module was increased by 40.17%. The vertical arrangement of the heat pipe showed better temperature control and equalization effects than the horizontal arrangement, reducing the maximum temperature difference by 32.7%. When the mass fraction of EG was 16.06%, the comprehensive performance was optimal, with the maximum temperature of the module under high thermal load at 54.14 °C and the maximum temperature difference controlled within 5 °C. The economic analysis showed that the payback period of the pure passive system was 1.77 years, and the return on investment over a 5-year service cycle was 182.6%, providing a reference for the engineering application of high-rate passive battery thermal management.

Peng et al. [14] developed and validated a three-dimensional numerical model for a cylindrical lithium-ion battery module with a compact hybrid cooling system of phase change material (PCM) and heat pipes. The PCM process and its effect on battery thermal behavior were numerically investigated for cases based on different discharge processes under varying thermal loads, different PCM properties (different mass fractions of expandable graphite), and different charge-discharge cycles of the battery module. The results indicated that the PCM liquid fraction distribution was not uniform during the discharge process; the PCM started to melt from its outermost neighboring the batteries, and its upper part became more liquid due to natural advection of liquid PCM. The different melting rates within the PCM led to a slightly enlarged temperature difference between batteries, and increasing discharge C-rate further accentuated this temperature difference. A tested composite PCM of 12 wt% EG (expanded graphite) showed better heat dissipation performance than that of pure PCM, and consequently it was better suited for battery thermal management systems. The simulations for different charge-discharge cycles indicated that lowering the thermal load and increasing recovery time could improve the thermal



[ Downloaded from ahc.iust.ac.ir on 2026-11-28 ]

performance of the battery module, making thermal control more effective. This study was particularly valuable for small or medium-sized cylindrical lithium-ion battery modules or packs, such as those used in electric bicycles and scooters, and provided detailed insights into the PCM melting and solidification processes and their effect on battery thermal behavior.

Despite the aforementioned advances in PCM-HP hybrid battery thermal management systems, several critical research gaps remain. First, most existing studies focus on conventional thermal loads and small-to-medium-capacity cells, while the thermal behavior and failure boundaries of PCM-HP hybrid systems under high heat flux conditions, as well as for large-capacity batteries (≥100 Ah), are not sufficiently understood [12], [13]. Second, the synergistic effects of key design parameters—such as HP arrangement orientation, expanded graphite content, PCM thickness, and copper foam porosity—on the coupled heat transfer mechanism have not been systematically quantified [10], [13], [14]. Third, the existing literature predominantly evaluates thermal performance metrics alone, lacking comprehensive technical and economic analyses from a whole-lifecycle perspective that could justify the practical investment in BTMS for battery life extension [13]. Fourth, the applicability boundaries of PCM-HP hybrid systems under combined high-temperature conditions remain unclear, and guidance for selecting appropriate hybrid configurations based on operational scenarios is limited [10], [14].

In view of these research gaps, it is worth noting that, among the limited number of studies in the literature, the combined utilization of composite phase change materials (CPCM) and heat pipes (HP) has been adopted only in a few references, and a systematic understanding of their synergistic thermal management mechanisms remains insufficient. The present work aims to provide a comprehensive investigation into the thermal performance, and practical applicability of PCM-HP hybrid BTMS for lithium-ion batteries. The specific objectives are: (1) to evaluate the cooling effectiveness of PCM-HP coupling systems under high-temperature conditions; (2) to develop and validate numerical models that can accurately predict the thermal behavior of the hybrid system. The findings of this study are expected to offer valuable insights for the design and optimization of Passive battery thermal management systems, particularly for high-power and large-capacity battery applications in Electric vehicles and Energy storage systems.

## 2. Numerical Method

### 2.1. Computational Domain

The computational domain was developed to numerically investigate the thermal performance of a battery cooling system integrated with a copper-foam/paraffin/resin composite and a heat pipe as shown in Figure 1. The composite is configured to match the dimensions of the prismatic cells. The cells are positioned adjacent to the composite and on both sides of the cooling system.

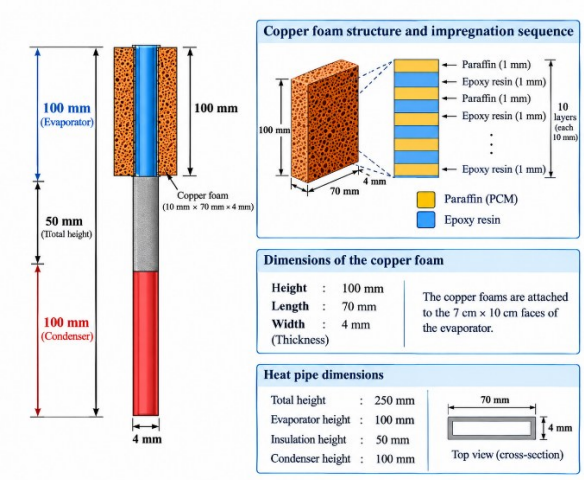


**Figure 1**: Schematic of proposed novel battery thermal management system

The cooling structure consists of a porous copper foam impregnated with RT38 paraffin and an epoxy resin matrix. The copper foam/PCM composite is positioned in thermal contact with the battery cell, while a heat pipe is incorporated into the cooling system to transfer the absorbed heat toward the condenser section.



[ Downloaded from ahc.iust.ac.ir on 2026-11-28 ]

The geometric and porous characteristics of the copper foam considered in the present study are summarized in Table 1.

The porous structure is assumed to be completely impregnated with RT38 paraffin and ML-506 epoxy resin layer by layer. The PCM absorbs the heat generated by the battery through sensible heating and latent heat during the phase-change process. The thermophysical properties of RT38 paraffin and the relevant properties and preparation conditions of the epoxy resin used in the numerical model are presented in Table 1. The melting temperature range of the PCM is 34–39 °C, which makes it suitable for controlling the battery temperature within the desired operating range.

**Table 1:** The properties and characteristics of composite

| | Parameter/ Property | Value |
|---|---|---|
| Copper foam | Porosity | 70–80% |
| | Pore density | 5–120 PPI |
| | Bulk density | 0.15–0.45 g/cm³ |
| | Length × width | 100 × 70 mm |
| | Thickness | 4–6 mm |
| RT38 paraffin | Melting temperature range | 34–39 °C |
| | Specific heat capacity | 2 kJ/(kg·K) |
| | Solid density | 0.88 kg/L |
| | Thermal conductivity | 0.2 W/(m·K) |
| | Maximum operating temperature | 70 °C |
| ML-506 epoxy | Physical state | Liquid |
| | Appearance | Light yellow |
| | Density at 25 °C | 1.11 g/cm³ |
| | Viscosity at 25 °C | 1450 Centipoise |
| | Resin-to-hardener mass ratio | 100:15 |
| | Mixing time | 3 min |

A heat pipe was incorporated into the cooling system to enhance heat removal from the battery and PCM composite. The heat pipe has a total length of 250 mm, comprising a 100-mm-long evaporator section located adjacent to the foam, a 50-mm-long adiabatic section for heat transfer, and a 100-mm-long condenser section for heat rejection. Its cross-sectional dimensions are 4 × 4 mm. The geometric parameters of the heat pipe are summarized in Table 2. In order to reduce computational effort and take advantage of symmetry, only half of the geometry is included in the computational domain.

**Table 2:** Geometric parameters of the heat pipe

| Parameter | Value |
|---|---|
| Width | 4 mm |
| Height | 4 mm |
| Total length | 250 mm |
| Evaporator length | 100 mm |
| Adiabatic section length | 50 mm |
| Condenser length | 100 mm |
| Effective thermal conductivity ($k_{eff}$) | 3870 W/(m·K) |

It should be noted that the heat pipe is assumed to operate within its capillary limit and boiling limit throughout the entire simulation period. The capillary limit corresponds to the maximum heat transport capacity that the wick structure can sustain without dry-out, while the boiling limit represents the maximum heat flux that can be accommodated at the evaporator without film boiling. In the present study, the imposed heat fluxes (1000–5000 W/m²) and the resulting thermal loads are well below these limits, ensuring that the heat pipe operates in a stable and reliable regime. Consequently, no dry-out condition, wick depletion, or boiling crisis is considered in the numerical model. The heat pipe is therefore treated as a passive heat-transport device with a constant effective thermal conductivity, as described in Section 2.2.

[ Downloaded from ahc.iust.ac.ir on 2026-11-28 ]

## 2.2. Governing Equations

Simulation and analysis of the three-dimensional model was carried out in ANSYS Fluent. The thermal behavior of the proposed model [9] is described by the heat transfer equation 1.

$$\rho_b C_{p,b} \frac{\partial T_b}{\partial t} = \nabla.(k_b \nabla T_b) + \dot{q} \quad (1)$$

where $\rho_b$ is the battery density, $C_{p,b}$ is the specific heat capacity, $k_b$ is the thermal conductivity (anisotropic for prismatic cells), and $\dot{q}$ is the volumetric heat generation rate.

Modeling is solely on the proposed composite, and the generated heat is defined as a boundary condition. Therefore, the sentence "heat generation" is zero.

For the CPCM, the enthalpy-porosity method is employed to model the phase change process according to equation 2.

$$H = h + \Delta H \quad (2)$$

where $h = h_{ref} + \int_{T_{ref}}^{T} C_p dT$ is the sensible enthalpy, and ΔH=βL is the latent enthalpy, with β being the liquid fraction and L the latent heat of fusion.

The copper foam was impregnated layer-by-layer with RT38 paraffin and ML-506 epoxy resin. The epoxy resin serves two engineering purposes: (i) mechanical encapsulation and structural integrity of the composite, and (ii) leakage prevention of the molten PCM during repeated melting/solidification cycles. Although the epoxy resin has a relatively low thermal conductivity, its presence is essential for the practical applicability of the composite.

In the numerical model, the layered composite was discretized as a multi-domain solid. Each paraffin layer and each epoxy-resin layer was treated as a separate solid sub-domain with its own thermophysical properties, and the energy equation was solved separately in each sub-domain with conjugate heat transfer at the interfaces. The layered geometry was resolved directly in the computational mesh, rather than being volume-averaged. This approach allows the model to capture the local thermal gradients between the paraffin and epoxy layers, which is essential for accurate prediction of the transient thermal response of the composite.

For the heat pipe, the apparent thermal resistance is defined as equation3.

$$R_{hp} = \frac{\bar{T}_e - \bar{T}_c}{Q_{in}}, \quad Q_{in} = q'' A \quad (3)$$

where:

- $\bar{T}_e$ is the average temperature of the evaporator section;
- $\bar{T}_c$ is the average temperature of the condenser section;
- $Q_{in}$ is the total heat input from the battery cell, which serves as the thermal load;
- $q''$is the heat flux imposed on the system from the battery cell;
- $A$ is the heat transfer area of cell.

It should be emphasized that the thermal resistance defined in Eq. (3) is an apparent transient thermal resistance of the overall system, not the intrinsic thermal resistance of the heat pipe alone. Under transient conditions, a portion of the applied heat load is stored as sensible and latent heat in the composite, and therefore the heat actually transported by the heat pipe is less than the total applied heat ($Q_{hp} < Q_{in}$). Consequently, the calculated resistance includes the effects of thermal energy storage in the PCM and the transient thermal response of the composite. This distinction is important for interpreting the non-monotonic behavior of $R_{hp}$observed in Figure 9.

In the present study, the heat pipe was modeled using the equivalent thermal conductivity (super-conductor) approach rather than resolving the transient two-phase flow within the vapor core and wick structure. This approach is justified by the fact that the primary objective of the present work is to evaluate the system-level thermal performance of the hybrid BTMS, rather than the internal two-phase dynamics of the heat pipe. The heat pipe was



[ Downloaded from ahc.iust.ac.ir on 2026-11-28 ]

therefore treated as a solid domain with an effective thermal conductivity of $k_{eff} = 3870\ W/(m.K)$, which is representative of copper-water heat pipes operating within their capillary and boiling limits. The evaporator, adiabatic, and condenser sections were assigned uniform effective properties, and no dry-out condition was considered.

### 2.3. Boundary and Initial Conditions

The boundary conditions were defined according to the physical configuration of the proposed thermal management system. Heat generated by the battery cell was introduced into the computational domain through the surface in contact with the copper-foam/PCM composite. Therefore, a prescribed heat flux was applied to the battery-side surface.

The lateral surfaces of the cooling structure were assumed to be adiabatic, thereby preventing heat loss through the side walls. The exposed portion of the heat pipe between the evaporator and condenser sections was also considered thermally insulated. Consequently, heat rejection from the system was assumed to occur only through the condenser section of the heat pipe. A convective boundary condition was applied to the condenser surface to represent heat transfer from the heat pipe to the surrounding environment. The initial temperature of the entire computational domain was set to 298.15 K (25 °C).

### 2.4. Simulated Cases for Parametric Study

To evaluate the thermal performance of the proposed cooling system under different thermal loads and heat-rejection conditions, both the applied heat flux and the convective heat-transfer coefficient at the condenser were varied. Three heat-flux levels of 1000, 2000, and 5000 W/m² were considered to represent different battery heat-generation conditions.

In addition, three values of the convective heat-transfer coefficient, namely 5, 50, and 500 W/(m²·K), were imposed at the condenser surface. These values represent different levels of heat-rejection capability from the heat pipe to the surrounding environment. Combining the three heat-flux levels with the three heat-transfer coefficients resulted in nine simulation cases, as summarized in Table 3.

**Table 3:** Case studies

| Case study | Applied heat flux, $q''$ (W/m²) | Condenser heat-transfer coefficient, $h$ (W/m²·K) |
|---|---|---|
| 1 | 1000 | 5 |
| 2 | 1000 | 50 |
| 3 | 1000 | 500 |
| 4 | 2000 | 5 |
| 5 | 2000 | 50 |
| 6 | 2000 | 500 |
| 7 | 5000 | 5 |
| 8 | 5000 | 50 |
| 9 | 5000 | 500 |

A grid and time-step independence study was performed to ensure the numerical accuracy of the present simulations. Three mesh sizes were tested: coarse (~250,000 cells), medium (~580,000 cells), and fine (~1,200,000 cells). The mesh quality was evaluated using the orthogonal quality criterion, with a minimum value of 0.15 and an average value of 0.82. The convergence criteria were set to $10^{-6}$ for the energy equation and $10^{-5}$ for the continuity and momentum equations. Three time steps were also tested: 0.1 s, 0.5 s, and 1.0 s. Table 4 summarizes the mesh and time-step configurations along with the resulting cell mean temperature at t = 600 s. As shown in Table 4, the cell mean temperature changes by less than 0.5 K when moving from the medium mesh to the fine mesh, and by less than 0.5 K when reducing the time step from 0.5 s to 0.1 s. Based on this study, the medium mesh (580,000 cells) and a time step of 0.5 s were selected for all



[ Downloaded from ahc.iust.ac.ir on 2026-11-28 ]

subsequent simulations, as they provide a satisfactory balance between numerical accuracy and computational cost.

**Table 4:** Mesh and time-step independence study: cell mean temperature at t = 600 s for different mesh sizes and time steps

| Mesh / Δt | Cells / Time step | Cell mean temperature at t = 600 s (K) |
|---|---|---|
| Mesh 1 (Coarse) | ~250,000 | 314.8 |
| Mesh 2 (Medium) | ~580,000 | 312.9 |
| Mesh 3 (Fine) | ~1,200,000 | 312.4 |
| Δt = 1.0 s | — | 313.6 |
| Δt = 0.5 s | — | 312.9 |
| Δt = 0.1 s | — | 312.4 |

## 2.5. Validation of the PCM Melting Model

The numerical model for PCM melting was validated against the experimental data of Katsman [16] and the numerical results of Shmueli et al. [15]. The validation case consists of a vertical cylindrical container (3 cm in diameter and 20 cm in height) initially filled with PCM to 85% of its volume. The container wall temperature was set 10 °C above the mean melting temperature of the PCM. The liquid fraction at 60-second intervals is compared in **Error! Reference source not found.**. As shown, the present simulation results agree very well with the experimental data up to t = 25 min. Beyond t = 25 min, a slight deviation is observed, not exceeding 8%.

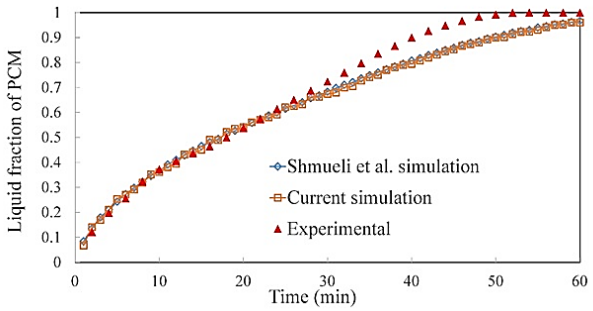


**Figure 2:** Validation of the numerical method with the experimental data [16]; the results of another numerical simulation [15] are also illustrated.

It should be noted that the present validation is limited to the PCM melting model. The heat pipe was modeled using the equivalent thermal conductivity approach, and its performance was not separately validated against experimental data. Similarly, the copper-foam composite was modeled using effective thermophysical properties, and its validation is beyond the scope of the present work. The validation presented here therefore confirms the accuracy of the phase-change model only, which is the fundamental physical model governing the thermal response of the composite.

## 3. Results and discussion

Before discussing the results, it is useful to establish the operating limits of lithium-ion batteries. The recommended upper limit for cell temperature is typically 348-353 K, while the recommended limit for temperature non-uniformity is approximately 303 K. These limits serve as reference points for evaluating the thermal performance of the proposed BTMS. In the following discussion, the observed thermal behavior is interpreted in light of these limits.

Figure 3 presents the variation of the cell mean temperature as a function of flow time for three different heat fluxes of 1000, 2000, and 5000 W/m². At the beginning of the simulation, the average temperature is approximately 300 K for all three cases, with negligible differences among them. As time progresses, the effect of



[ Downloaded from ahc.iust.ac.ir on 2026-11-28 ]

heat flux on the thermal response of the system becomes increasingly evident. At a heat flux of 1000 W/m², the average temperature initially increases and subsequently remains nearly constant, reaching approximately 310 K at the end of the simulation period. Increasing the heat flux to 2000 W/m² results in a more pronounced temperature rise, with the average temperature reaching approximately 330 K. In contrast, at the highest heat flux of 5000 W/m², a substantially steeper temperature increase is observed, and the average temperature reaches nearly 400 K at the end of the simulation.

This behavior can be attributed primarily to the higher rate of thermal energy input at increased heat fluxes. Although the heat transfer and thermal storage mechanisms provided by the heat pipe and the paraffin-based composite can effectively limit the temperature rise at lower heat fluxes, their ability to maintain a low and relatively stable temperature becomes increasingly constrained as the imposed heat flux increases. The considerably higher temperature rise observed at heat flux of 5000 W/m² therefore indicates that the thermal load imposed on the system exceeds the rate at which heat can be effectively transferred and/or stored under the investigated conditions. Nevertheless, the specific contribution of the paraffin phase-change process to this thermal behavior cannot be determined solely from this figure. Therefore, the average paraffin temperature and liquid fraction should be considered together to further clarify the role of latent heat storage in regulating the temperature of the system.

Figure 4 compares the temporal variation of the average temperature of the cell surface and composite for heat transfer coefficients of h=50 and 500 W/(m²·K) and for three imposed heat fluxes of 1000, 2000, and 5000 W/m². At h=50, the temperature increase becomes increasingly pronounced with increasing heat flux. For q"=1000 W/m², the average temperature remains relatively stable after the initial transient period and reaches approximately 310–311 K at the end of the simulation. Increasing the heat flux to 2000 W/m² results in a higher final temperature of approximately 320–321 K. The most significant temperature rise occurs at q"=5000W/m², for which the average temperature increases continuously and reaches approximately 365 K.

In contrast, a substantial reduction in temperature is observed when the heat transfer coefficient is increased from h=50 to h=500 W/(m²·K). At h=500 W/(m²·K), the final average temperatures for q"=1000, 2000, and 5000 W/m^2 are approximately 301.5, 305, and 315 K, respectively. Particularly, for the highest heat flux of 5000 W/m², increasing the heat transfer coefficient results in a reduction of approximately 50 K in the final average temperature compared with the h=50 W/(m²·K) case.

The pronounced reduction in temperature with increasing h can be attributed to the enhanced convective heat transfer from the cell–composite system to the surroundings. A higher heat transfer coefficient increases the heat removal capability of the system and consequently reduces the thermal accumulation within the cell and composite. This effect becomes more significant at higher heat fluxes, where the thermal load imposed on the system is considerably greater. Therefore, the results demonstrate that increasing the heat transfer coefficient can substantially improve the thermal regulation capability of the proposed system, particularly under high heat-flux conditions.

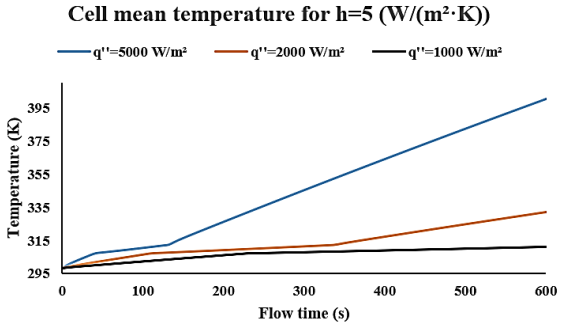


**Figure 3:** The cell mean temperature for heat transfer coefficients of h=5 W/(m²·K)



[ Downloaded from ahc.iust.ac.ir on 2026-11-28 ]

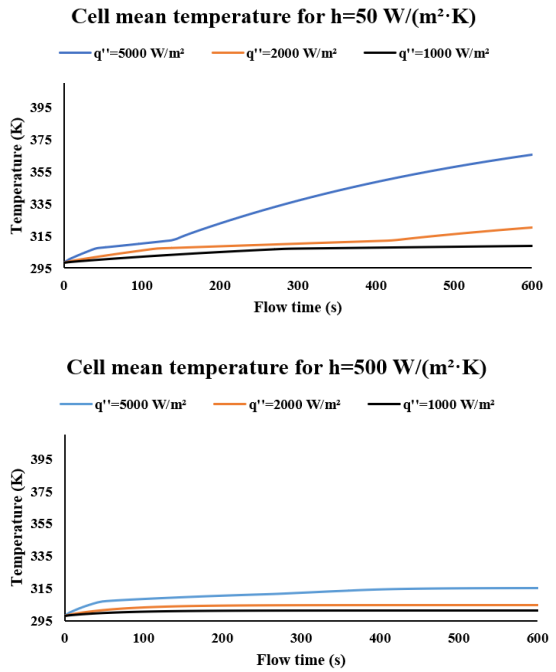


**Figure 4:** The cell mean temperature for heat transfer coefficients of h=50 and h=500 W/(m²·K)

It should be noted, however, that the temperature response alone does not provide sufficient information to quantify the contribution of the paraffin phase-change process. The corresponding paraffin temperature and liquid-fraction profiles should therefore be analyzed to determine whether the lower temperatures obtained at higher h are accompanied by a reduction in the melting rate and latent-heat utilization.

At $q'' = 5000\ W/m^2$ and $h = 5\ W/(m^2 \cdot K)$, the maximum cell temperature reached approximately 400 K, which is well above the recommended upper limit of 348-353 K for lithium-ion batteries. This indicates that at low convective heat-transfer coefficients, the proposed BTMS alone is insufficient to maintain the battery within a safe operating range under extreme heat fluxes, and supplementary active cooling may be required. In contrast, at $h = 500\ W/(m^2 \cdot K)$, the maximum cell temperature remained below 315 K even at $q'' = 5000\ W/m^2$, demonstrating the critical role of effective external cooling in maintaining battery safety.

Figure 5 illustrates the variation of the average composite temperature with flow time for three heat fluxes of 1000, 2000, and 5000 W/m² under different heat transfer coefficients. A clear dependence of the composite temperature on both the imposed heat flux and the heat transfer coefficient can be observed. At the lowest heat transfer coefficient, h=5 W/(m²·K), increasing the heat flux results in a substantial increase in the composite temperature. In particular, for q"=5000 W/m², the composite temperature continuously increases and reaches approximately 400 K at the end of the simulation, whereas the corresponding temperatures for q"=2000 and 1000 W/m² remain at approximately 330 and 310 K, respectively.

Increasing the heat transfer coefficient to h=50 W/(m²·K) considerably reduces the temperature rise of the composite, particularly at the highest heat flux. For q"=5000W/m², the final composite temperature decreases to approximately 365 K. A further increase in the heat transfer coefficient to h=500 W/(m²·K) results in a pronounced reduction in the composite temperature. Under this condition, the final temperatures for q"=1000, 2000, and 5000 W/m² are approximately 301–302, 305, and 315 K, respectively.

The results demonstrate that increasing the heat transfer coefficient significantly enhances the heat removal capability of the thermal management system. This effect becomes particularly important at high heat fluxes, where the rate of heat input is sufficiently large to cause substantial thermal accumulation when the heat transfer coefficient is low. For example, at q"=5000 W/m², increasing h from 5 to 500W/(m²·K) reduces the final composite temperature by approximately 85 K. This pronounced reduction indicates that enhancing the external heat transfer capability can effectively suppress thermal accumulation within the composite and maintain a considerably lower operating temperature.

The temperature behavior observed here is also consistent with the previously discussed



[ Downloaded from ahc.iust.ac.ir on 2026-11-28 ]

cell-surface temperature results, confirming the strong influence of the heat transfer coefficient on the thermal response of the system. However, the effect of this temperature reduction on the phase-change behavior of the paraffin cannot be established from the composite temperature alone. Therefore, the corresponding paraffin temperature and liquid-fraction profiles are required to determine the extent of melting and the associated utilization of latent heat.

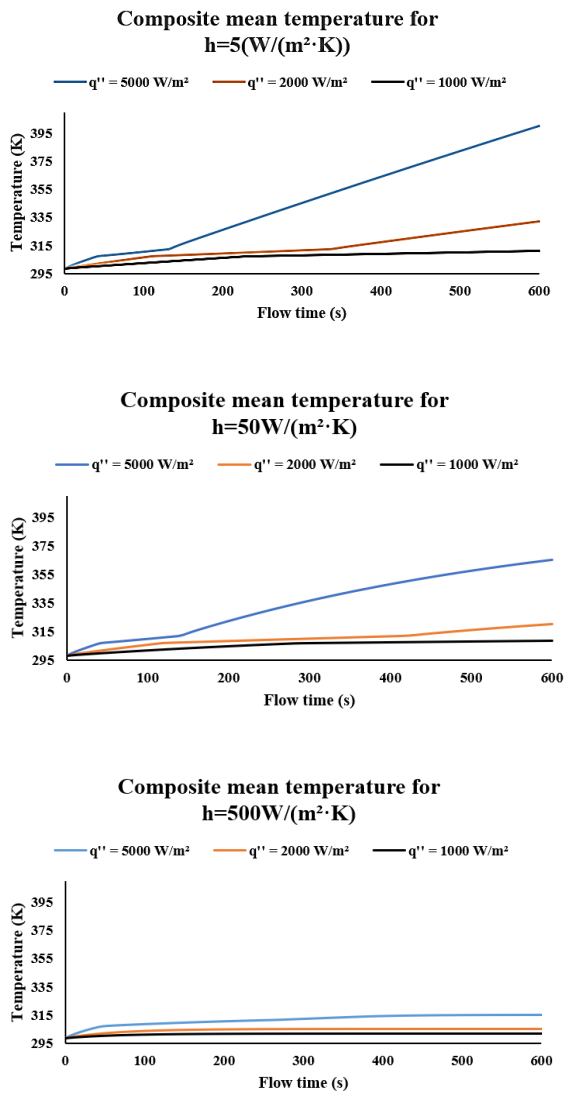


**Figure 5:** The average temperature of the composite for heat transfer coefficients of h=5, h=50 and h=500 W/(m²·K)

Figure 6 presents the temporal variation of the maximum temperature difference between the cell surface and the composite under different heat fluxes and heat transfer coefficients. In general, the maximum temperature difference increases with increasing heat flux, indicating the development of stronger thermal gradients between the cell and the composite under higher thermal loads.

At h=5W/(m²·K), the temperature difference remains relatively small at q"=1000W/m² and decreases to approximately 0.1 K at the end of the simulation. For q"=2000 W/m², a non-monotonic behavior is observed, with the temperature difference initially increasing, followed by a reduction and a subsequent increase to approximately 0.55 K. The largest temperature difference occurs at q"=5000 W/m², reaching approximately 1.4 K at the end of the simulation.

A similar dependence on heat flux is observed for h=50 and h=500. W/(m²·K) At h=50W/(m²·K), the final maximum temperature difference increases from approximately 0.3 K at q"=1000 W/m² to about 0.8 K and 2.3 K at q"=2000 and 5000W/m², respectively. For the highest heat transfer coefficient, h=500 W/(m²·K), the temperature difference reaches approximately 0.6, 1.2, and 3.0 K for heat fluxes of 1000, 2000, and 5000 W/m², respectively.

An important observation is that increasing the heat transfer coefficient substantially reduces the average temperature of the cell–composite system, as discussed previously, while the maximum temperature difference between the cell surface and the composite may increase, particularly at high heat fluxes. This indicates that a lower average temperature does not necessarily correspond to improved temperature uniformity. The enhanced heat removal at higher values of h may cause the composite to respond more rapidly to the external cooling conditions, while the cell surface remains directly subjected to the imposed heat flux, thereby resulting in a larger temperature gradient between the two regions. Therefore, the thermal performance of the proposed system should be evaluated based on both the reduction of the average temperature and the control of temperature non-uniformity.



[ Downloaded from ahc.iust.ac.ir on 2026-11-28 ]

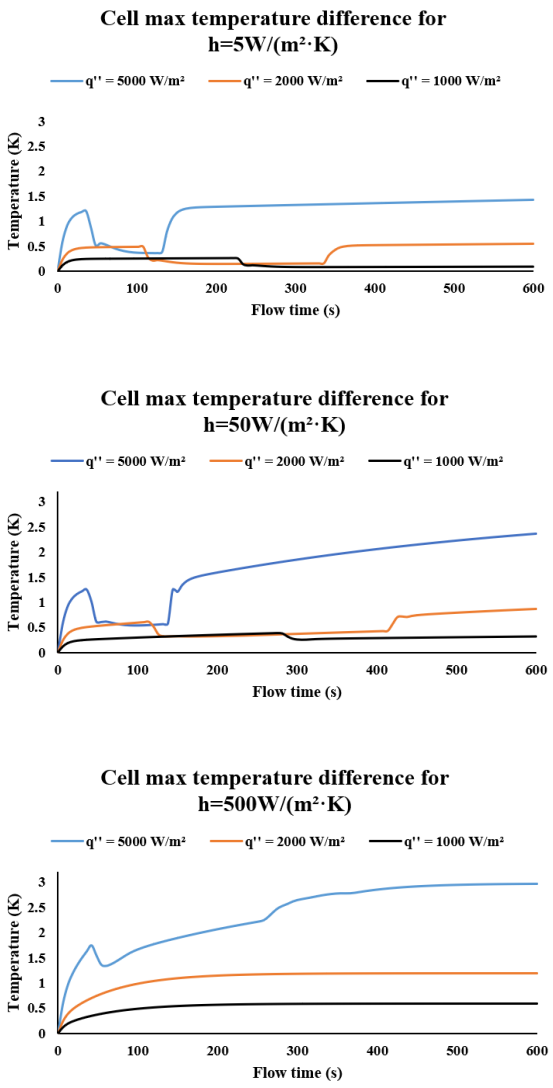


**Figure 6:** The maximum temperature difference between the cell and the composite for heat transfer coefficients of h=5, h=50 and h=500 W/(m²·K)

Figure 7 illustrates the temporal evolution of the mean temperature of the paraffin layers saturated copper foam for different heat-transfer coefficients of the heat pipe and imposed heat fluxes. A clear dependence of the PCM thermal response on both the heat flux and the heat-transfer coefficient is observed. At a low heat-transfer coefficient of $h = 5$ W/(m²·K), increasing the heat flux from 1000 to 5000 W/m² results in a substantial increase in the PCM mean temperature. In particular, the mean temperature at $q'' = 5000$ W/m² reaches approximately 400 K after 600 s, compared with approximately 330 and 310 K for $q = 2000$ and 1000 W/m², respectively. This pronounced temperature increase at high heat flux indicates that the heat-removal capability of the heat pipe is insufficient to effectively dissipate the imposed thermal load when the heat-transfer coefficient is relatively low.

Increasing the heat-transfer coefficient from 5 to 50 W/(m²·K) significantly improves the thermal response, particularly at the highest heat flux. At $q'' = 5000$ W/m², the final mean temperature decreases from approximately 400 to 365 K. A smaller reduction is observed for $q = 2000$ W/m², while the effect of increasing $h$ is relatively limited at $q = 1000$ W/m². This behavior indicates that the influence of the heat-transfer coefficient becomes increasingly important as the imposed heat flux increases, because a higher thermal load requires a greater heat-removal rate through the heat pipe.

The most pronounced thermal improvement is obtained at $h = 500$ W/(m²·K). Under this condition, the mean PCM temperature remains relatively low for all investigated heat fluxes, reaching approximately 315, 305, and 301–302 K for $q'' = 5000$, 2000, and 1000 W/m², respectively. For the highest heat flux, increasing $h$ from 5 to 500 W/(m²·K) reduces the temperature rise after 600 s from approximately 100 K to only 17 K. This substantial reduction demonstrates the critical role of the heat pipe in providing an efficient heat-removal pathway from the porous PCM composite.

The gradual reduction in the temperature growth rate observed in the curves can also be attributed to the thermal buffering provided by the paraffin-based PCM. During phase transition, a considerable portion of the supplied thermal energy can be stored as latent heat, thereby limiting the sensible temperature increase of the composite. The combination of PCM latent-heat storage and enhanced heat removal through the heat pipe is particularly effective at high values of $h$, resulting in improved temperature regulation. Overall, the



[ Downloaded from ahc.iust.ac.ir on 2026-11-28 ]

results demonstrate that increasing the heat-transfer coefficient is an effective strategy for mitigating PCM temperature rise, especially under high heat-flux conditions.

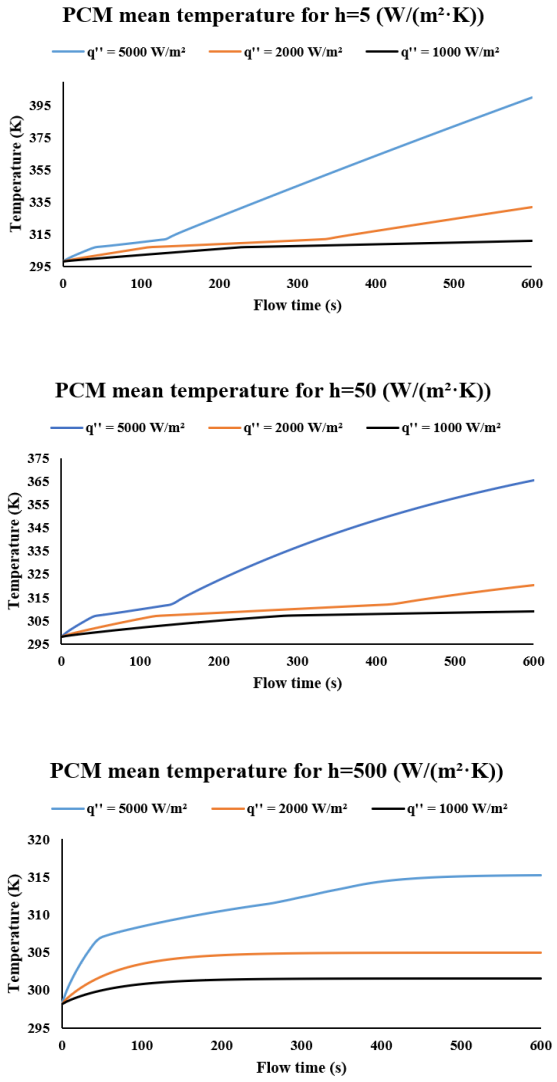


**Figure 7:** The average temperature of the PCM layers in the composite for heat transfer coefficients of h=5, h=50 and h=500 W/(m²·K)

Figure 8 illustrates the temporal evolution of the liquid fraction of the paraffin PCM embedded in the copper foam for different imposed heat fluxes and heat-transfer coefficients of the embedded heat pipe. A pronounced dependence of the melting behavior on the applied heat flux is observed. Increasing the heat flux from 1000 to 5000 W/m² substantially accelerates PCM melting. For $h = 5\ W/(m^2K)$, the liquid fraction reaches unity at approximately 140 s, 340 s, and beyond 600 s for $q'' = 5000$, 2000, and 1000 W/m², respectively. At $q = 1000\ W/m^2$, the liquid fraction reaches approximately 0.78 at 600 s, demonstrating that the PCM remains partially melted within the investigated period.

The results further reveal an interesting influence of the heat-transfer coefficient of the heat pipe. Increasing $h$ from 5 to 50 W/(m²K) delays the melting process at the lower heat fluxes. For $q = 2000\ W/m^2$, the complete melting time increases from approximately 340 to 430 s, whereas for $q = 1000\ W/m^2$, the liquid fraction at 600 s decreases from approximately 0.78 to 0.35. This behavior can be attributed to the enhanced thermal coupling between the heat pipe and the composite at higher $h$, which increases the heat-removal capability of the heat pipe and consequently reduces the fraction of the supplied thermal energy available for PCM melting. The influence of $h$, however, becomes considerably less pronounced at $q'' = 5000\ W/m^2$, where the high imposed heat flux dominates the thermal response and complete melting occurs within approximately 140–150 s. These results indicate that the melting dynamics are governed by the competition between the imposed thermal input and the heat extraction capacity of the heat pipe.

Figure 9 illustrates the variation of the apparent thermal resistance of heat pipe at heat transfer coefficient of $h = 5, 50\ and\ 500\ \mathrm{W/(m^2 \cdot K)}$. Three heat fluxes of 1000, 2000, and 5000 W/m² were considered.

In $h = 5\ \mathrm{W/(m^2 \cdot K)}$ the apparent thermal resistance for all three heat flux values begins to increase rapidly. The magnitude of this initial response strongly depends on the applied heat flux. At $q'' = 5000$ W/m², the apparent thermal resistance reaches a pronounced maximum of approximately 0.07 K/W within the first several tens of seconds. Subsequently, it decreases



[ Downloaded from ahc.iust.ac.ir on 2026-11-28 ]

significantly and approaches approximately 0.02–0.03 K/W. A similar, although less pronounced, behavior is observed at $q'' = 2000$ W/m².

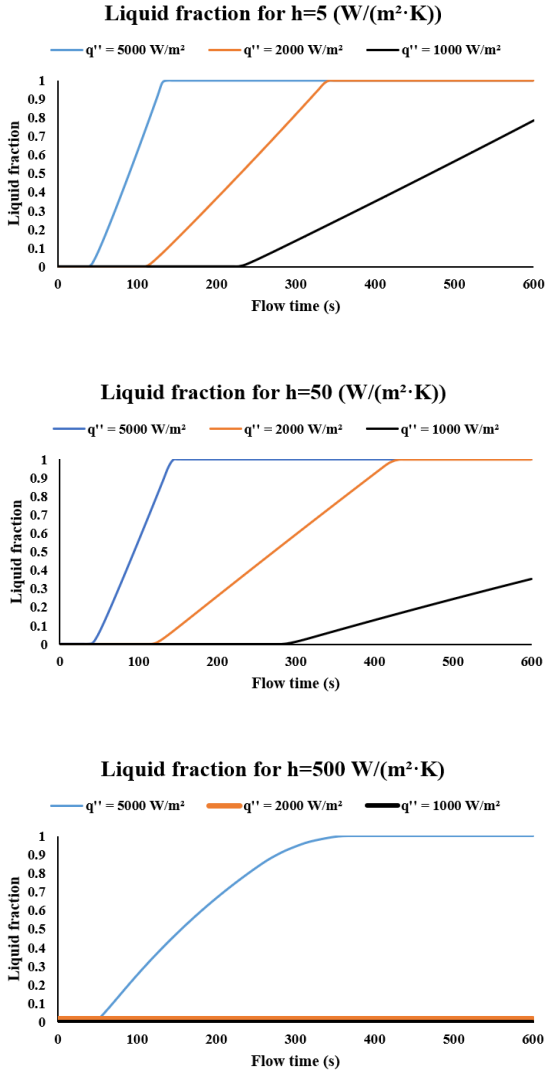


**Figure 8:** Liquid fraction of the PCM layers in the composite for heat transfer coefficients of h=5, h=50 and h=500 W/(m²·K)

The decrease in apparent thermal resistance after the initial peak can be attributed to the activation of the phase-change process. As the paraffin approaches its melting temperature, a considerable portion of the supplied thermal energy is absorbed as latent heat rather than producing a proportional increase in temperature. Consequently, the temperature rise is temporarily suppressed, leading to a reduction in the apparent thermal resistance. This behavior demonstrates the beneficial thermal buffering capability of the paraffin-filled copper foam.

The copper foam plays an important role during this process by providing a highly conductive metallic network within the phase-change material. In combination with the heat pipe, this conductive structure facilitates heat spreading and promotes a more uniform distribution of thermal energy throughout the composite. Therefore, the PCM does not act independently; rather, the copper foam and heat pipe provide efficient heat transport pathways while the paraffin provides thermal storage through latent heat absorption.

After approximately 120–150 s, the apparent thermal resistance increases again, particularly for the highest heat flux. This second increase indicates that the latent-heat storage capability of the PCM gradually becomes less effective as the melting process progresses. Once a significant fraction of the paraffin has melted, further heat input produces a greater temperature increase, resulting in a continuous increase in the apparent thermal resistance. At $q'' = 5000$ W/m², this increase is considerably stronger than that observed at 1000 and 2000 W/m², reaching approximately 0.08–0.09 K/W toward the end of the test.

At the lowest heat flux of 1000 W/m², the apparent thermal resistance remains relatively low and stable, with only minor variations during the entire test period. This indicates that the lower heat input allows the PCM to absorb the supplied energy more effectively and delays the exhaustion of its latent-heat capacity.

At $h = 50$ W/(m² · K). Compared with the $h = 5$ W/(m² · K) case, the overall evolution of the curves is smoother, particularly at the intermediate and low heat fluxes. for $q'' = 5000$ W/m², the apparent thermal resistance initially increases



[ Downloaded from ahc.iust.ac.ir on 2026-11-28 ]

to approximately 0.07–0.08 K/W, followed by a reduction to approximately 0.04 K/W. This reduction again corresponds to the period in which the PCM undergoes significant melting and latent heat absorption. After this period, the apparent thermal resistance increases progressively and reaches approximately 0.16–0.17 K/W at 600 s. The pronounced increase at high heat flux indicates that the available latent-heat capacity becomes insufficient to maintain the temperature rise at a low level over the entire test duration. at $q'' = 2000$ W/m², the initial peak is substantially lower, followed by a decrease to approximately 0.025 K/W. The subsequent increase is relatively gradual, reaching approximately 0.06 K/W at the end of the experiment. The 1000 W/m² case exhibits the smallest variation, with the apparent thermal resistance remaining close to 0.02–0.025 K/W.

In contrast to the two lower-convection cases, the curves of $h = 500$ W/(m² · K) exhibit a much smoother evolution, and the sharp fluctuations observed at $h = 5$ and 50 W/(m² · K) are significantly reduced. for $q'' = 5000$ W/m², the apparent thermal resistance increases rapidly during the initial stage and reaches approximately 0.12 K/W. A small decrease is then observed, followed by a continuous increase. The apparent thermal resistance eventually approaches approximately 0.21 K/W after 400–500 s. The relatively smooth increase suggests that the thermal response is governed by the combined effects of composite, heat-pipe and progressive evolution of the PCM state. at $q'' = 2000$ W/m², the apparent thermal resistance increases rapidly during the early stage and gradually approaches approximately 0.08–0.085 K/W. In comparison, the 1000 W/m² case reaches a substantially lower quasi-steady value of approximately 0.04–0.045 K/W.

The strong dependence of apparent thermal resistance on heat flux at $h = 500$ W/(m² · K) indicates that the system response becomes increasingly nonlinear at high heat flux. The higher heat input causes a greater temperature difference across the system and accelerates the thermal evolution of the PCM. Nevertheless, the absence of severe oscillations or abrupt transitions at this condition indicates a more stable thermal response compared with the lower-$h$ cases.

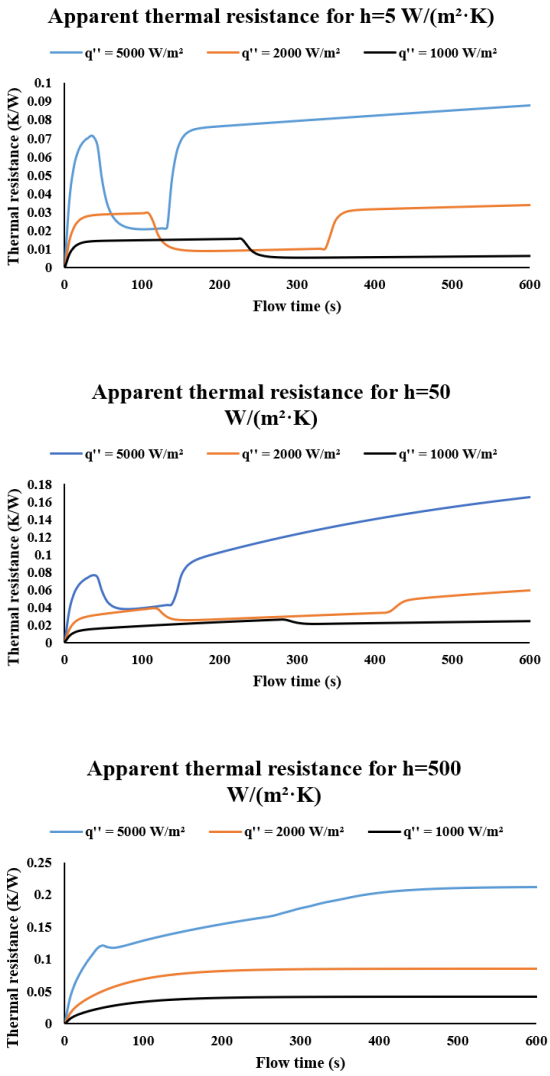


**Figure 9:** Apparent thermal resistance of the heat pipe for heat transfer coefficients of h=5, h=50 and h=500 W/(m²·K)

The thermal behavior observed in this study can be interpreted as a competition between three mechanisms: heat generation by the battery, latent heat absorption by the PCM, and heat transport by the heat pipe. In the early stage of heating (t < 50 s), heat generation dominates, leading to a rapid temperature rise. As the



[ Downloaded from ahc.iust.ac.ir on 2026-11-28 ]

paraffin approaches its melting range (50 s < t < 150 s), latent heat absorption becomes dominant, which significantly reduces the rate of temperature increase. After complete melting (t > 150 s), the heat pipe becomes the primary heat-removal pathway, and the temperature increases gradually. This competition explains the non-monotonic behavior of the apparent thermal resistance observed in Figure 9.

The transient behavior of the apparent thermal resistance can be divided into three distinct regimes: (i) an initial rapid increase due to sensible heating of the composite; (ii) a decrease associated with latent heat absorption during PCM melting; and (iii) a subsequent increase after complete melting, when the PCM no longer provides effective thermal buffering. This three-regime behavior is more pronounced at higher heat fluxes, where the PCM melting process is accelerated.

## 4. Conclusion

In this study, the thermal performance of a hybrid battery thermal management system consisting of a paraffin-based composite and a heat pipe was numerically investigated under different heat fluxes and convective heat transfer coefficients. The effects of these parameters on cell and composite temperatures, temperature uniformity, PCM phase change, and apparent thermal resistance were evaluated. The main conclusions are as follows:

1. Heat flux strongly influenced the thermal response of the system. Increasing the heat flux from 1000 to 5000 W/m² increased the average temperatures of the cell surface and composite and accelerated PCM melting. At higher thermal loads, the demand on the heat pipe also increased.
2. Increasing the convective heat transfer coefficient enhanced heat removal. Increasing h from 5 to 500 W/(m²·K) reduced the average temperatures of both the cell and composite, with the most pronounced effect observed at q" = 5000 W/m². Thus, stronger convective cooling effectively suppressed thermal accumulation.
3. Temperature uniformity depended on both heat flux and cooling conditions. The maximum temperature difference between the cell surface and composite generally increased with heat flux. Therefore, BTMS performance should be assessed using both the absolute temperature level and temperature uniformity rather than average temperature alone.
4. PCM utilization was strongly dependent on heat flux. At h = 50 W/(m²·K), increasing q" from 1000 to 5000 W/m² advanced the onset of melting from approximately 290 to 45 s. At q" = 5000 W/m², complete melting occurred at approximately 145 s, whereas at 2000 W/m² it occurred around 440 s. At 1000 W/m², only about 35% of the PCM melted by 600 s, indicating that a substantial latent-heat storage capacity remained available.
5. The combined analysis of temperature, liquid fraction, and apparent thermal resistance provides a more comprehensive assessment of system performance. Higher heat fluxes accelerate PCM melting and increase thermal demand, whereas higher h enhances heat rejection and limits temperature rise. The results demonstrate that the coupled effects of PCM phase change and heat-pipe heat transport play a key role in the thermal behavior of the proposed hybrid BTMS.

The results indicate that the proposed configuration can effectively mitigate temperature rise under the investigated thermal loading conditions.

## Reference

[1] G. Hekimoğlu and A. Sarı, “A review on phase change materials (PCMs) for thermal energy storage implementations,” *Mater. Today Proc.*, vol. 58, pp. 1360–1367, Jan. 2022, doi: 10.1016/j.matpr.2022.02.231.

[2] M. H. Nahani, G. R. Molaeimanesh, and M. Dahmardeh, “Evaluating the Performance and Environmental Impact of Electric Vehicles



[ Downloaded from ahc.iust.ac.ir on 2026-11-28 ]

with Old Battery Pack: A Well-to-Wheel Analysis," *Automotive Science and Engineering*, vol. 14, no. 4, 2024, doi: 10.22068/ase.2024.683.

[3] H. Liu, Z. Wei, W. He, and J. Zhao, "Thermal issues about Li-ion batteries and recent progress in battery thermal management systems: A review," 2017, *Elsevier Ltd*. doi: 10.1016/j.enconman.2017.08.016.

[4] S. Jenabi Haqparast, G. R. Molaeimanesh, and S. M. Mousavi-Khoshdel, "Role of phase change materials in creating uniform surface temperature on a lithium battery cell applicable in electric vehicles," *Automotive Science and Engineering*, vol. 8, no. 4, 2018, doi: 10.22068/ijae.8.4.2848.

[5] A. Ansari Laleh and M. H. shojaeefard, "A Comprehensive Review of Phase Change Materials and Their Application in Thermal Management Systems of Lithium-ion Batteries," *Automotive Science and Engineering*, vol. 14, no. 4, 2024, doi: 10.22068/ase.2024.695.

[6] M. Zhi *et al.*, "Recent research progress on phase change materials for thermal management of lithium-ion batteries," Jan. 01, 2022, *Elsevier Ltd*. doi: 10.1016/j.est.2021.103694.

[7] Y. Zhang, J. Huang, M. Cao, G. Du, Z. Liu, and L. wang, "A novel sandwich structured phase change material with well impact energy absorption performance for Li-ion battery application," *J. Energy Storage*, vol. 40, Aug. 2021, doi: 10.1016/j.est.2021.102769.

[8] C. Lv *et al.*, "Experimental investigation of permeability and Darcy-Forchheimer flow transition in metal foam with high pore density," *Exp. Therm. Fluid Sci.*, vol. 154, May 2024, doi: 10.1016/j.expthermflusci.2024.111149.

[9] Y. Salami Ranjbaran, M. H. Shoajeefard, and G. R. Molaeimanesh, "Thermal behavior of a commercial prismatic Lithium-ion battery cell applied in electric vehicles," *Automotive Science and Engineering*, vol. 8, no. 2, 2018, doi: 10.22068/ijae.8.2.2700.

[10] R. Feng, P. Huang, Z. Tang, Y. He, and Z. Bai, "Experimental and numerical study on the cooling performance of heat pipe assisted composite phase change material-based battery thermal management system," *Energy Convers. Manag.*, vol. 272, p. 116359, 2022, doi: https://doi.org/10.1016/j.enconman.2022.116359.

[11] Z. Tang, R. Feng, P. Huang, Z. Bai, and Q. Wang, "Modeling analysis on the cooling efficiency of composite phase change material-heat pipe coupling system in battery pack," *J. Loss Prev. Process Ind.*, vol. 78, p. 104829, 2022, doi: https://doi.org/10.1016/j.jlp.2022.104829.

[12] H. Zhao *et al.*, "Thermal management of 500 Ah large-capacity lithium-ion battery and module with composite phase-change materials and heat pipes: An experimental and simulation study," *J. Energy Storage*, vol. 125, p. 116862, 2025, doi: https://doi.org/10.1016/j.est.2025.116862.

[13] Y. Zhang, H. Wang, X. Cui, and Y. Wang, "Heat pipe-composite PCM coupled battery thermal management: High-rate thermal optimization and life-cycle economic evaluation," *International Journal of Thermal Sciences*, vol. 230, p. 111214, 2026, doi: https://doi.org/10.1016/j.ijthermalsci.2026.111214.

[14] P. Peng, Y. Wang, and F. Jiang, "Numerical study of PCM thermal behavior of a novel PCM-heat pipe combined system for Li-ion battery thermal management," *Appl. Therm. Eng.*, vol. 209, p. 118293, 2022, doi: https://doi.org/10.1016/j.applthermaleng.2022.118293.

[15] H. Shmueli, G. Ziskind, and R. Letan, "Melting in a vertical cylindrical tube: Numerical investigation and comparison with experiments," *Int. J. Heat Mass Transf.*, vol. 53, no. 19, pp. 4082–4091, 2010, doi: https://doi.org/10.1016/j.ijheatmasstransfer.2010.05.028.

[ Downloaded from ahc.iust.ac.ir on 2026-11-28 ]

[16] Katsman L, "Investigation of phase change in cylindrical geometry with internal fins," Negev, 2006.

[ Downloaded from ahc.iust.ac.ir on 2026-11-28 ]